
DiscDiff: Latent Diffusion Model for DNA Sequence Generation

Zehui Li¹ Yuhao Ni² William A V Beardall¹
 Guoxuan Xia² Akashaditya Das¹ Tim August B. Huygelen³ Guy-Bart Stan¹ Yiren Zhao²

Abstract

This paper introduces a novel framework for DNA sequence generation, comprising two key components: DiscDiff, a Latent Diffusion Model (LDM) tailored for generating discrete DNA sequences, and Absorb-Escape, a post-training algorithm designed to refine these sequences. Absorb-Escape enhances the realism of the generated sequences by correcting ‘round errors’ inherent in the conversion process between latent and input spaces. Our approach not only sets new standards in DNA sequence generation but also demonstrates superior performance over existing diffusion models, in generating both short and long DNA sequences. Additionally, we introduce EPD-GenDNA, the first comprehensive, multi-species dataset for DNA generation, encompassing 160,000 unique sequences from 15 species. We hope this study will advance the generative modelling of DNA, with potential implications for gene therapy and protein production.

1. Introduction

Diffusion Models (DMs) are emerging as a promising tool in the field of protein design – models using structural (Watson et al., 2023) and amino acid sequence level data have produced state-of-the-art results (Alamdari et al., 2023). On the other hand, the application of DMs for DNA generation remains limited. Well-designed synthetic DNA sequences are vital for enhancing gene therapies tasks (Liu et al., 2022), such as the control of gene expressions in complex genetic circuits (Zrimec et al., 2022) and the production of novel proteins (Gupta & Zou, 2019). However, research in applying deep learning to these important tasks is heavily limited by the absence of extensive datasets for DNA generation,

well-defined evaluation metrics, and robust baseline models.

Prior work on DNA generation has used Generative Adversarial Networks (GANs) (Goodfellow et al., 2014) for the generation of synthetic DNA sequences (Killoran et al., 2017; Wang et al., 2020; Zrimec et al., 2022). However, it has been shown that the generated samples lack diversity (Dhariwal & Nichol, 2021) and suffer from mode collapse at training time (Metz et al., 2016). To address these issues, Diffusion Models (DMs) have been proposed, which iteratively refine sample quality. Despite their effectiveness, the discrete nature of DNA sequences poses a unique challenge for standard DMs, traditionally designed for vision data. This has led to the development of specialized variants like the Dirichlet Diffusion Score Model (DDSM) (Avdeyev et al., 2023) and EvoDiff (Alamdari et al., 2023), tailored for discrete biological sequence generation. These models employ diffusion-like processes to modify discrete data, although they are computationally intensive, as discussed by (Salimans et al., 2017).

In an attempt to mitigate computational demands, Latent Diffusion Models (LDMs) have been introduced, utilizing a compressed and regularized latent space to reduce complexity. However, current LDMs for discrete data (Dieleman et al., 2022; Li et al., 2022; Han et al., 2022) are mainly domain-specific and not directly applicable to DNA sequences. A significant challenge in adapting LDMs for discrete data generation lies in mitigating ‘rounding errors’ during conversions between the latent and input spaces. Such errors can lead to inaccuracy, especially in long sequences. This problem has been evident in text generation, where LDMs often produce less fluent sentences compared to autoregressive models (Zhang et al., 2023).

This study introduces a novel learning framework for DNA sequence generation. It consists of: 1) DiscDiff - an LDM for generating discrete sequences and 2) Absorb-Escape - a post-training algorithm to refine sequences generated by the LDM. DiscDiff contains a new network architecture for mapping discrete sequences to continuous latent spaces and vice versa. Absorb-Escape, on the other hand, is a novel inference framework that combines the strengths of LDMs and autoregressive models. Absorb-Escape scans through the generated sequences, and actively corrects

¹Department of Bioengineering, Imperial College London ²Department of Electrical and Electronic Engineering, Imperial College London ³University College London. Correspondence to: Zehui Li <zl6222@ic.ac.uk>, Guy-Bart Stan <g.stan@imperial.ac.uk>, Yiren Zhao <a.zhao@imperial.ac.uk>.

Table 1. A comparison of DNA generation datasets, our EPD-GenDNA is significantly larger in size and contains more species.

Dataset	# DNA	Species	Seq. Len.
EPD-GenDNA (Ours)	160k	15	2048&256
DDSM (Avdeyev et al., 2023)	100k	Human	1024
ExpGAN (Zrimec et al., 2022)	4238	Yeast	1000
EnhancerDesign (Taskiran et al., 2023)	7770	Human	500

Table 2. A comparison of DNA generation algorithms, our DiscDiff is the first LDM approach that is tested on various species.

Algorithm	Type	Regulatory/Protein Encoding Regions	MultiSpecies
DiscDiff (Ours)	LDMs	Both	✓
DDSM (Avdeyev et al., 2023)	DMs	Both	✗
ExpGAN (Zrimec et al., 2022)	GANs	Regulatory	✗
EnhancerDesign (Taskiran et al., 2023)	GANs	Regulatory	✗
FeedbackGAN (Gupta & Zou, 2019)	GANs	Protein Encoding	✗

these ‘rounding errors’, thus producing more realistic samples. As shown in Figure 1, while DiscDiff by itself has achieved state-of-the-art results in DNA sequence generation, Absorb-Escape further improves the quality of the generated DNA sequences. In addition, to fully evaluate the potential of these techniques, we propose the first large-scale cross-species dataset for DNA generation, with defined metrics and tasks to benchmark generative models on DNA synthesis. Our contributions are as follows:

- We introduce EPD-GenDNA, a dataset built on EPD (Meylan et al., 2020). As shown in Table 1, it is the first comprehensive, multi-species, multi-cell type dataset for DNA generation. The dataset encompasses 160,000 unique DNA sequences, derived from 15 species, covering 2,713 cell types, and is based on 300 million wet lab experiments.
- We propose *DiscDiff*, to our best knowledge, the first application of Latent Diffusion Models (LDMs) to the task of DNA generation. DiscDiff surpasses existing state-of-the-art diffusion models in short and long DNA generation by 7.6% and 1.9%, respectively, as measured by the motif distribution.
- We propose *Absorb-Escape*, a generalisable post-training algorithm for refining the quality of generated discrete sequences. We show that Absorb-Escape further increases the performance of DiscDiff by 4% in long DNA generation. In addition, Absorb-Escape allows control over the property of generated samples.
- Lastly, we demonstrate a practical application of DNA generative modelling. We train a conditional generative model capable of realistically simulating regulatory elements and genes across 15 species.

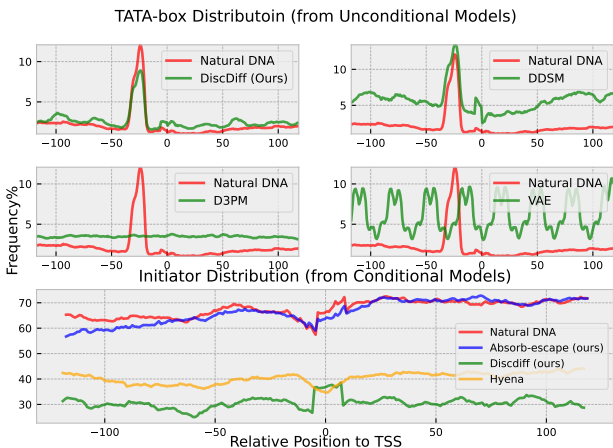


Figure 1. A comparison of Motif frequency distributions. The graphs contrast the occurrences of TATA-Box and Initiator motifs at each position in a set of samples from natural DNA against those generated by various models. A close match in frequency distributions suggests a higher realism and better performance for the generated DNA sequences. **DiscDiff and Absorb-Escape outperform existing models qualitatively by a significant margin.**

2. Related Work

Diffusion Models (DMs). Initially proposed by (Sohl-Dickstein et al., 2015), two parallel perspectives of diffusion models have been developed. In the probabilistic denoising view (Ho et al., 2020), a forward diffusion process gradually adds noise to the input data x_0 , and a reverse diffusion process gradually removes the noise from the perturbed data x_t .

The reverse denoising (generative) process is parameterized with a trainable network $\mu_\theta(x_t, t)$. $\mu_\theta(x_t, t)$ is either a U-Net (Ronneberger et al., 2015) or a Transformer (Gupta et al., 2023) with free parameters, and is trained via evidence lower bound (ELBO) or denoising score matching loss.

An alternative perspective involves modelling diffusion as stochastic differential equations (SDE) and their respective inverse processes. (Song et al., 2020b). This formulation allows the use of ODE solvers to compute the reverse process efficiently (Song et al., 2020a; Lu et al., 2022; Zhang & Chen, 2023; Xia et al., 2023). In this work, we will follow the denoising view of the diffusion model, and use a reparameterising trick found in Latent Diffusion Models (Rombach et al., 2022). In this notation, the training process can also be interpreted as training a noise predictor ε_θ :

$$\min_{\theta} \mathbb{E}_{x, t \sim U[1, T], \varepsilon \sim \mathcal{N}(0, 1)} [\|\varepsilon - \varepsilon_\theta(x_t, t)\|_2^2]. \quad (1)$$

Latent Diffusion Models (LDMs). LDMs convert discrete inputs into a continuous latent space. This technique is widely employed in language modelling, where

text is transformed into a continuous format using tools like word2vec or neural network-based embeddings (Dieleman et al., 2022; Li et al., 2022; Han et al., 2022). Diffusion-like processes can be applied to discrete data (Avdeyev et al., 2023), but LDMs are preferred for their computational efficiency - this is due to the compaction and smoothness of the latent space (Rombach et al., 2022). Current state-of-the-art models are usually domain-specific and rely on pre-trained language models to form latent embeddings (Lovelace et al., 2022; Zhang et al., 2023). Additionally, discrete generation using diffusion models often encounters rounding errors when mapping from the latent space to text tokens (Zhang et al., 2023; Li et al., 2022; Lin et al., 2022). Similar issues arise in the generation of DNA sequences. Specifically, the accumulation of rounding errors can result in the production of invalid DNA sequences, this effect is more prominent in the generation of longer sequences.

In contrast, autoregressive models learn the conditional probability of the next token based on previous ones. This generally results in more locally coherent samples. Such models have been successfully used in text generation (Radford et al., 2019; Brown et al., 2020; Touvron et al., 2023) and genomic sequence modeling (Lal et al., 2023; Ji et al., 2021; Dalla-Torre et al., 2023; Nguyen et al., 2023). However, autoregressive models can accumulate errors over time, leading to repetitive and overly confident outputs (Xu et al., 2022). They generate samples with lower diversity than diffusion models (Lovelace et al., 2022), which is detrimental to genome sequence generation, where diversity is a key metric.

While there are works aiming to combine the advantages of diffusion and autoregressive models (Zhang et al., 2023; Xu et al., 2022), they rely on existing autoregressive language models, which have the same time and space complexity as the original autoregressive models. In this work, we propose a novel algorithm, the *Absorb-Escape* algorithm, which can be applied to any diffusion model to improve the local coherency of generated samples.

Deep Generative Models for DNA Sequences The primary goal of DNA generation is to produce *realistic* regulatory elements or genes. Regulatory elements (Eraslan et al., 2019) are specific DNA sequences that control gene expression, whereas genes encode proteins. Generative adversarial networks (GANs) have been used for DNA sequence creation. This includes the creation of protein-encoding region (Wang et al., 2020), enhancer (Taskiran et al., 2023) and promoter sequences (Zrimec et al., 2022).

While diffusion models for DNA generation are less explored, one recent work Dirichlet Diffusion Score Model (DDSM) (Avdeyev et al., 2023) uses the Dirichlet distribution in the discrete diffusion process. DDSM also

compares its performance against other discrete DMs, such as BitDiffusion (Chen et al., 2022) and D3PM (Austin et al., 2021) on the human DNA generation task. However, DDSM primarily focuses on conditional generation, where a real-valued vector of the same length as the input sequence is used for conditioning. This approach simplifies the DNA generation problem, due to the large amount of conditional information available for each sample.

Large autoregressive models have also been adopted for learning DNA sequence representations (Ji et al., 2021; Dalla-Torre et al., 2023; Nguyen et al., 2023). This includes transformer-based models (Ji et al., 2021; Dalla-Torre et al., 2023) and state-space models (Nguyen et al., 2023; Lal et al., 2023; Gu & Dao, 2023). Notably, state-space models with fewer parameters can outperform transformer-based architectures in both genomics classification and regression tasks (Gu & Dao, 2023).

The development of generative algorithms for DNA sequences has significant challenges, primarily due to the scarcity of well-formatted data and effective evaluation metrics. While existing datasets support regulatory element (Grešová et al., 2023), species classification (Mock et al., 2022), and genomic assay prediction (Kelley et al., 2018; Avsec et al., 2021), prior DNA generation efforts have been limited by small, single-species datasets (Zrimec et al., 2022; Wang et al., 2020; Avdeyev et al., 2023; Killoran et al., 2017). Although motif distribution plots have been used for evaluating the property of the generated DNA sequences, there is a lack of metrics available to quantitatively measure the quality of generated sequences.

To address this gap, our study extends the current analysis meta to include a comparative evaluation between autoregressive and diffusion models for DNA sequence generation. We explore the unconditional and conditional generation of long and short DNA sequences. We assess the effectiveness of the generation process using models trained on a comprehensive, large-scale dataset and analyse their performance using quantitative metrics. This work provides a thorough method for the comparison of generative models in the DNA generation space and advances the field.

3. Generation Task with EPD-GenDNA

We present EPD-GenDNA, a novel multi-species DNA sequence dataset, originating from the Eukaryotic Promoter Database (EPDnew) (Meylan et al., 2020). This extensive dataset includes manually curated and authenticated DNA sequences, along with comprehensive annotations specifying species and cell types for each sequence. Incorrect annotations were filtered out, with detailed preprocessing steps described in Appendix A.

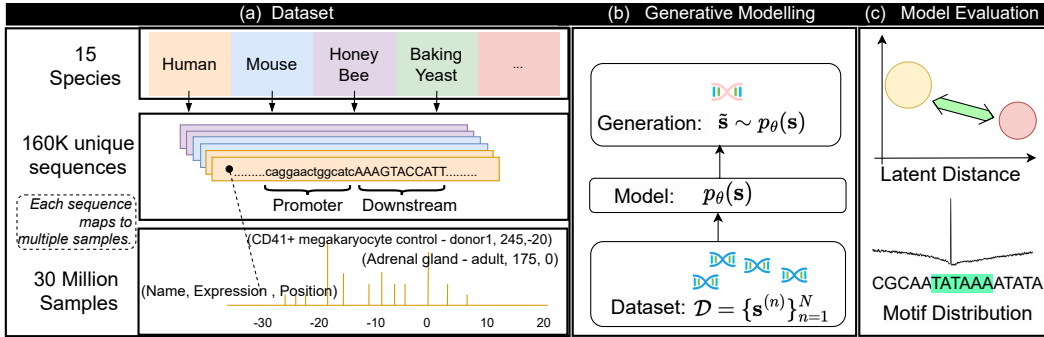


Figure 2. Generation Task with EPD-GenDNA. **(a) Dataset:** The EPD-GenDNA dataset includes 160K unique sequences from 15 species and 30 million samples with associated metadata. **(b) Generative Modelling:** A probabilistic model $p_{\theta}(s)$ is trained to generate new DNA sequences. **(c) Model Evaluation:** Generated sequences are evaluated through measuring latent distances and analyzing motif distributions.

Dataset Format As shown in Figure 2, EPD-GenDNA includes 160K unique (promoter, gene) pairs across 15 species, covering a significant portion of known mammalian promoters (Périer et al., 1998). The dataset spans 30 million samples, each associated with metadata like sample names, cell types, and expression levels, detailed in Table 7 in Appendix A. We present two versions of the dataset with different sequence lengths. 1) **EPD-GenDNA-small:** 256-base window centered on a gene’s transcription start site, split into upstream promoter and downstream segment. 2) **EPD-GenDNA-large:** 2048-base window centered on a gene’s transcription start site, for broader genetic regions.

While the small version is suitable for single regulatory elements and small gene generation, the large version is more suitable for the generation of multiple regulatory elements and large genes. Let $\mathbb{N}_4 = \{1, 2, 3, 4\}$ where each element represents one of the four nucleotides in a DNA sequence, specifically, adenine (A), thymine (T), guanine (G), and cytosine (C). Then, a DNA sequence of length L can be represented as $s \in \mathbb{N}_4^L$. In the above datasets, L is 256 and 2048, respectively.

The Unconditional Generation Task We work with a dataset of real-world DNA sequences $\mathcal{D} = \{s^{(n)}\}_{n=1}^N$ collected from some distribution $p(s)$, where each sequence $s^{(n)} \in \mathbb{N}_4^L$ represents a chain of nucleotides. $L = 256$ for EPD-GenDNA-small and $L = 2048$ for EPD-GenDNA-large. The objective is to develop a generative model $p_{\theta}(s)$ of the data distribution $p(s)$ from which we can sample novel sequences $\tilde{s} \sim p_{\theta}(s)$. These sequences should be structured arrangements of A, T, G, and C, reflecting the complex patterns found in actual DNA.

The Conditional Generation Task The conditional generation task involves generating DNA sequences given specific conditions or attributes. Here, the dataset of DNA sequences $\mathcal{D} = \{s^{(n)}, c^{(n)}\}_{n=1}^N$ is sampled from the joint distribution

$p(s, c)$, where c represents the condition associated with each sequence. The conditions could include species type, expression level, or cell types, adding a layer of specificity to the generation process. The objective in this task is to develop a model $p_{\theta}(s|c)$ that generates new DNA sequences \tilde{s} given condition c . In this paper, we focus on conditioning DNA generation with the species of the organism.

Evaluation Metrics For the evaluation of generated DNA sequences, the following metrics are used:

1. **Motif Distribution Correlation (Cor_M):** The motifs are small sequences carrying biological significance. And motif distribution is the frequency distribution of the motif along the length of a set of DNA sequences. As shown in Figure 1, motif distributions of the generated DNA sequences should be similar to the real DNA sequences. More precisely, Cor_M measures the correlation between generated and natural DNA sequences for specific motifs frequency, where $M \in \{\text{TATA-box, GC-box, Initiator, CCAAT-box}\}$. The correlation is defined as the Pearson correlation between the motif distributions of generated and natural DNA sets.
2. **Diversity:** Defined as $\prod_{n=10}^{12} \frac{|f_{\text{count}}(n, \mathcal{D})|}{f_{\text{count}}(n, \mathcal{D})}$, where f_{count} counts the number of n-grams in a set of generated DNA sequences \mathcal{D} , and $|f_{\text{count}}(n, \mathcal{D})|$ is the unique number of n-grams. This metric assesses the variety within the generated DNA sequences.
3. **S-FID (Sei Fréchet Inception Distance):** Adapted from the Fréchet Inception Distance used in image generation (Heusel et al., 2017), S-FID metric measures the distance between the distributions of generated and natural DNA sequences in the latent space. It uses the encoder of a pre-trained genomic neural network, Sei (Zhou & Troyanskaya, 2015), to map the DNA sequence into the latent space.

4. Method

4.1. The DiscDiff Model

We introduce DiscDiff, a novel, and to our knowledge the first Latent Discrete Diffusion model for DNA generation tasks. As shown in Figure 3, this model is structured into two main components: a Variational-Auto-Encoder (VAE) and a denoising model. The VAE consists of an encoder $\mathbf{E} : s \mapsto z$, which maps discrete input sequence s to a continuous latent variable z , and a decoder $\mathbf{D} : z \mapsto \tilde{s}$, which reverts z back to \tilde{s} in the discrete space. The denoising model $\varepsilon_\theta(z_t, t)$ is trained to predict the added noise ε in the latent space.

4.1.1. VAE ARCHITECTURE

The choice of VAE architecture in LDMs is critical and often domain-specific. For example, Stable Diffusion (Romach et al., 2022) uses a hybrid architecture that combines convolutional neural networks (CNNs) and 2d-attention for image generation, while PLANNER (Zhang et al., 2023) and LD4LG (Lovell et al., 2022) use transformer-based architectures for text generation.

Three types of encoders have been widely used in genomic sequence modelling: CNNs with pooling layers (Alipanahi et al., 2015; Kelley et al., 2018; Kelley, 2020), CNNs with self-attention (Avsec et al., 2021), and 1D-Swin (Li et al., 2023). In this work, we design three autoencoders based on these architecture variants. Namely, we have CNN-VAE, CNN-Attn-VAE, and 1D-Swin-VAE. Furthermore, we find that mapping the input data to a higher dimension space can help to learn a better denoising network, generating more realistic DNA sequences as shown in the ablation study of Section 5.1. We hereby propose to use a two-stage VAE architecture as shown in Figure 3.

The first stage encoder $\mathbf{E}_{\phi_1} : \mathbb{N}_4^L \rightarrow \mathbb{R}^{K \times M}$ maps $s \in \mathbb{N}_4^L$ to a 2D latent space $z_1 \in \mathbb{R}^{K \times M}$, where K is the number of channels and M is the length of the latent representation. The second stage encoder $\mathbf{E}_{\phi_2} : \mathbb{R}^{1 \times K \times M} \rightarrow \mathbb{R}^{C \times K' \times M'}$ first adds a dummy dimension to z_1 such that $z_1 \in \mathbb{R}^{1 \times K \times M}$ and then maps it to 3d latent space $z \in \mathbb{R}^{C \times K' \times M'}$, where C is the number of channels, K' and M' are the reduced dimensions of K and M respectively. The decoder in the first and second stage are \mathbf{D}_{θ_1} and \mathbf{D}_{θ_2} respectively. Which are symmetric to the encoders. Overall, we have $z = \mathbf{E}_\phi(s) = \mathbf{E}_{\phi_2}(\mathbf{E}_{\phi_1}(s))$, and the reconstruction is $\tilde{s} = \mathbf{D}_\theta(z) = \mathbf{D}_{\theta_1}(\mathbf{D}_{\theta_2}(z))$.

4.1.2. VAE LOSS

When training the VAE, we propose to use Cross Entropy (CE) as reconstruction loss. The loss function is given by:

$$\mathbf{L}_{\theta, \phi} = \underbrace{\mathbb{E}_{p(s)} \left[\mathbb{E}_{q_\phi(z|s)} \left[- \sum_{l=1}^L \sum_{i=1}^4 \delta_{i,s_l} \log p_\theta(s_l|z) \right] \right]}_{\text{Reconstruction Loss}} + \underbrace{\beta \cdot \mathbb{E}_{p(s)} [\text{KL}(q_\phi(z|s) || \mathcal{N}(z; \mu, \Sigma))]}_{\text{KL Divergence}}$$

where δ_{ij} is the Kronecker delta, $p_\theta(s|z)$ is the probabilistic decoder output from \mathbf{D}_θ ; $q_\phi(z|s)$ is the probabilistic output from encoder \mathbf{E}_ϕ that represents the approximate posterior of the latent variable z given the input s ; $\mathcal{N}(z; \mu, \Sigma)$ is the prior on z . Here we use a simple isotropic. β is a mixing hyperparameter.

4.1.3. DENOISING NETWORK TRAINING

Once \mathbf{D}_θ and \mathbf{E}_ϕ are trained in the first step, we train a noise prediction ε_θ in the latent space $z = \mathbf{E}_\phi(s)$ with Equation (2). The details about the U-Net configuration can be found in Appendix C.

$$\mathbb{E}_{z, t \sim U[1, T], \varepsilon \sim \mathcal{N}(0, I)} [\|\varepsilon - \varepsilon_\theta(z_t, t)\|_2^2] \quad (2)$$

4.2. Absorb-Escape

Latent Diffusion Models (LDMs) may produce errors at the single nucleotide level during conversion from latent to input space. We hypothesise that these inaccuracies are reflected in lower softmax coefficients output by the model. As illustrated in Figure 4, these lower coefficients often cluster, forming noticeable ‘valleys’ in regions of the sequence with low probability.

To address this issue, we introduce the ‘Absorb-Escape’ algorithm, designed specifically to refine these problematic ‘valley’ areas. The intuition behind Absorb-Escape is that while the Latent Diffusion Models effectively capture the overall structure of the sequences, they tend to make mistake at a single nucleotide level.

This algorithm functions by detecting and amending these small-scale errors, thereby enhancing the overall accuracy of the generated sequences. For this refinement process, we utilize pre-trained autoregressive models, which are particularly effective in capturing local nuances and details of the sequences. This approach enables a more precise correction of the errors made by LDMs, resulting in sequences with improved accuracy both in local and global contexts.

Given a sequence s generated by a diffusion model \mathcal{D} and a pre-trained autoregressive model \mathcal{M} . We use $L(\mathcal{D}, s_i)$ and $L(\mathcal{M}, s_i)$ to represent the maximum softmax coefficient returned by two models at position i . The Absorb-Escape algorithm operates as follows, with absorb condition \mathcal{A} and escape condition \mathcal{E} defined in Table 3.

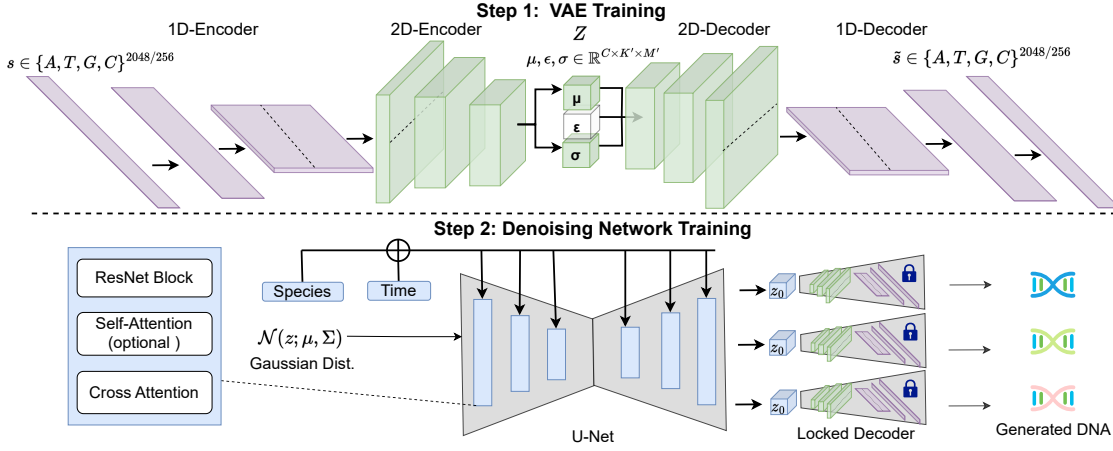


Figure 3. DiscDiff Model: A two-step process for DNA sequence generation. **Step 1: VAE Training:** A sequence $s \in \{A, T, G, C\}^{2048/256}$ is encoded via a 1D-Encoder to a 2D-Encoder. The latent space representation Z with parameters μ, ϵ, σ is then decoded back to \tilde{s} through a 2D-Decoder and 1D-Decoder. **Step 2: Denoising Network Training:** The latent representation Z is processed through a denoising network comprising a ResNet Block, optional Self-Attention, and Cross Attention, with species and time information. The network outputs a Gaussian distribution $N(z; \mu, \Sigma)$. A U-Net architecture takes this distribution to produce various z_0 representations, which a Locked Decoder (frozen parameters) used to generate the final DNA sequences.

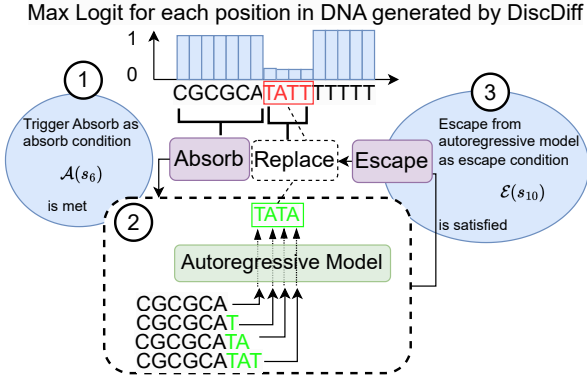


Figure 4. The Absorb-Escape Algorithm: Enhancing DNA Sequence Prediction. While diffusion models (DMs) effectively capture broad DNA sequence features, they can err at the single nucleotide level. The Absorb-Escape algorithm corrects such errors by identifying and modifying low probability nucleotides, like changing ‘TATT’ to ‘TATA’. This improves accuracy over using only DMs or autoregressive models, as shown in Figure 1.

- Absorb:** Iterate through each token $s_i \in s$. Check if the absorb condition $\mathcal{A}(s_i)$ is met. If $\mathcal{A}(s_i)$ is true, proceed to the next step.
- Autoregressive Generation:** Use a pretrained autoregressive model \mathcal{M} to refine the sequence starting from position i where $\mathcal{A}(s_i)$ is satisfied.
- Escape:** Continue the generation process until the

Table 3. Absorb and Escape Conditions. In these conditions, T_{absorb} represents the predefined absorb threshold. The escape threshold is indicated by T_{escape} , while T_{random} stands for the random threshold. Lastly, max_sub_length means the maximum subsequence length.

Type	Condition Name	Description
Absorb	Threshold Condition	$\mathcal{A}(s_i) = \text{true if } L(\mathcal{D}, s_i) < T_{\text{absorb}}$
	Natural	$\mathcal{E}(s_j) = \text{true if } L(\mathcal{D}, s_j) > L(\mathcal{M}, s_j)$
Escape	Threshold	$\mathcal{E}(s_j, T_{\text{escape}}) = \text{true if } L(\mathcal{M}, s_j) < T_{\text{escape}}$
	Random	$\mathcal{E}(s_j, T_{\text{random}}) = \text{true if } \text{rand.uniform}(0,1) > T_{\text{random}}$
	Max Length	$\mathcal{E}(s_j, \text{max_sub_length}) = \text{true if } j > \text{max_sub_length}$

escape condition $\mathcal{E}(s_j, \text{params})$ is satisfied. Replace the low probability region in the original sequence s with the newly generated sequence from \mathcal{M} .

When implementing the Absorb-Escape algorithm, various conditions and parameters can be selectively adjusted. Typically, we opt for the natural escape conditions (Table 3) by default. This choice enables the autoregressive model to iteratively enhance local inaccuracies, continuing this refinement process until the diffusion model reaches a state of confidence regarding its output.

5. Results and Evaluation

In Section 5.1, we conduct an ablation study to understand the impact of different components in DiscDiff. In Section 5.2, we compare DiscDiff with the baseline diffusion models on unconditional generations. Section 5.3 shows a comparison between DiscDiff and the autoregressive foundation model Hyena on conditional generations. We show that

Table 4. Ablation study: Comparison of different versions of DiscDiff on EPD-GenDNA-large.

Encode	Acc \uparrow	S-FID \downarrow	Cor _{TATA} \uparrow	Δ Div \downarrow
CNN-VAE	99.4%	45.2	0.858	4.2%
CNN-Attn-VAE	98.8%	53.6	0.531	9.8%
1D-Swin-VAE	99.6%	82.1	0.651	7.5%

the use of the Absorb-Escape algorithm can allow the user to trade-off between desired motifs in generated sequences.

5.1. Ablation Study

For the latent diffusion model, one important design choice is the architecture of the VAE. We train different VAE architectures on EPD-GenDNA-large and compare their performance on unconditional generation. During the first stage of training, three encoders: CNN-VAE, CNN-Attn-VAE, and 1D-Swin-VAE are trained to convergence.

We use the reconstruction accuracy of the VAEs as an evaluation metric in Table 4, which is defined as the percentage of the reconstructed sequence that is identical to the input sequence from the VAE. As shown by the first column of Table 4, 1D-Swin-VAE achieves the highest reconstruction accuracy, while CNN-Attn-VAE achieves the lowest reconstruction accuracy.

However, when evaluated on their sequence generation capability after using these VAEs in DiscDiff, CNN-VAE achieves the best performance as measured by S-FID and Cor_{TATA}. We then visualize the latent space of the VAEs by projecting it to 2D using UMAP (McInnes et al., 2018). We calculate the number of dimensions needed to explain the 95% of the variance. It is evident that 1D-Swin-VAE needs more dimensions to reach the 95% of the variance compared to CNN-VAE. Intuitively, this shows that CNN-VAE forms a simpler latent space than 1D-Swin-VAE. We hypothesize that this simpler latent space formulation significantly eases the subsequent training of the diffusion model. Detail and the visualizations are presented in Appendix D.

5.2. Unconditional Generation

First, we compare the performance of DiscDiff and other models on unconditional generation for mammalian DNA sequences and present the results in Table 5. The training set consists of 65,000 unique DNA sequences. We compare our model against the state-of-the-art discrete diffusion model: DDSM (Avdeyev et al., 2023), D3PM (Austin et al., 2021), and BitDiffusoin (Chen et al., 2022). For the autoregressive models used in Absorb-Escape, we fine-tune the pre-trained Hyena (Nguyen et al., 2023) on EPD-GenDNA-large and EPD-GenDNA-small. The training budget is fixed to 72 GPU-Hours on NVIDIA A100 for all models. Training details are found in Appendix E.

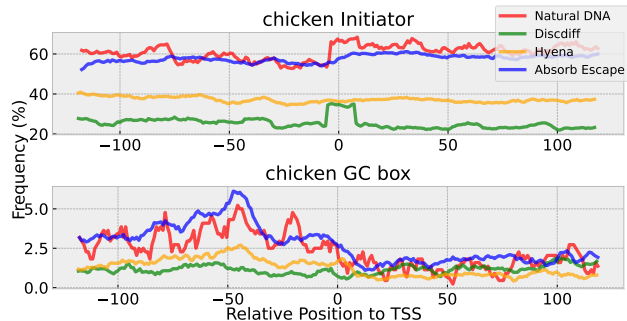


Figure 5. Model Comparison of Chicken DNA Motif Distributions. This illustrates the Initiator and GC box frequencies across natural and generated DNA sequences near the TSS.

A Comparison to other Diffusion Models We generated 50,000 samples from each model. Metrics measuring the generated sequences are detailed in Table 5. DiscDiff produces the most realistic DNA sequences compared to other diffusion baselines on both short and long-sequence generations. This is indicated by both the smallest latent distance (S-FID) and largest motif frequency correlation (Cor_{TATA}) scores when compared to the ground truth. For diversity, we want the generated sequence to have similar diversity to the training data. This means that generated sequences have diversity that matches natural diversity. We measure it by Δ Div, the diversity difference between natural and generated sequences. We see that D3PM (Large) has the smallest Δ Div but performs worse than DiscDiff when it comes latent distance and motif frequency correlation.

The Absorb-Escape Algorithm The Absorb-Escape algorithm, which refines generated sequences of DiscDiff with Hyena, boosts the quality of generated sequences: it significantly reduces the S-FID and achieves the highest correlation score among all the models. We also compare our model against Hyena (an autoregressive model) in Appendix F.

5.3. Conditional Generation Results

This section highlights the performance of DiscDiff in conditional DNA sequence generation. As shown in Figure 5, we apply the Absorb-Escape algorithm and see that it improves DiscDiff’s performance, particularly DiscDiff’s ability to generate DNA with desired motifs. Using a training set of 160,000 DNA sequences from 15 species, DiscDiff and Hyena were trained to generate 4,000 samples per species. We looked at the frequency and position of key genetic motifs in the generated samples (TATA-box, Initiator, GC-content, CCAAT-box). The full results are shown in Figure 10 to Figure 24 in Appendix G. When compared to Hyena, we saw that DiscDiff Escape algorithm was able to achieve better accuracy in trend replication

Table 5. A comparison of diffusion models on unconditional generation evaluated on EPD-GenDNA-small and EPD-GenDNA-large. Metrics include S-FID, Cor_{TATA} , and ΔDiv . The best and second-best scores are highlighted in bold and underlined, respectively.

Model	EPD-GenDNA-small			EPD-GenDNA-large		
	S-FID ↓	Cor_{TATA} ↑	ΔDiv ↓	S-FID ↓	Cor_{TATA} ↑	ΔDiv ↓
Random (Reference)	119.0	-0.241	29.3%	106.0	0.030	13.0%
Sample from Training Set	0.509	1.0	0	0.100	0.999	0
VAE	295.0	-0.167	<u>0.40%</u>	250.0	0.007	10.6%
BitDiffusion	405	0.058	44.9%	100.0	0.066	2.00%
D3PM (small)	97.4	0.0964	28.0%	94.5	0.363	12.8%
D3PM (large)	161.0	-0.208	0.10%	224.0	0.307	0.10%
DDSM (Time Dilation)	504.0	0.897	40.6%	1113.0	0.839	13.0%
DiscDiff (Ours)	<u>57.4</u>	<u>0.973</u>	4.40%	<u>45.2</u>	<u>0.858</u>	4.20%
Absorb-Escape (Ours)	3.21	0.975	5.70%	4.38	0.892	<u>1.90%</u>

Table 6. A performance comparison of models Hyena, DiscDiff, and Absorb-Escape on EPD-GenDNA-small for Baking Yeast and Fruit Fly. Models are evaluated on Cor_{TATA} and $Cor_{Initiator}$. Best scores are highlighted and averages across 15 species are provided. The species-specific results are presented in Tables 8 to 12.

Model	Baking Yeast		...	Fruit Fly		Average (15 Species)		
	Cor_{TATA} ↑	$Cor_{Initiator}$ ↑		Cor_{TATA} ↑	$Cor_{Initiator}$ ↑	Cor_{TATA} ↑	$Cor_{Initiator}$ ↑	$\frac{Cor_{TATA} + Cor_{Initiator}}{2}$ ↑
Hyena	0.958	0.723	...	0.970	0.198	0.939	0.488	0.714
DiscDiff	0.858	0.824	...	0.813	0.926	0.894	0.581	0.738
Absorb-Escape	0.864	0.902	...	0.937	0.630	0.917	0.568	0.743

of motif distributions. Employing the Absorb-Escape algorithm improves the quality of generated samples. The algorithm merges the strengths of both models and produces realistic samples in terms of the trend line and the frequency values as shown in Figure 5 – Absorb-Escape (blue) closely tracks the Natural DNA frequency distribution (red).

DiscDiff and Hyena are better suited for modelling different types of motifs. Table 6 shows that DiscDiff outperforms Hyena in modelling Initiator motifs, while Hyena outperforms DiscDiff in modelling TATA-box, as indicated by Cor_{TATA} and $Cor_{Initiator}$. Absorb-Escape combines the strength of both models, achieving the best performance in $\frac{Cor_{TATA} + Cor_{Initiator}}{2}$. Species-specific results can be found in Table 8 to Table 12.

Balancing Motifs with Absorb-Escape The Absorb-Escape algorithm offers control over the properties of generated sequences. Figure 6 shows that varying the absorb threshold biases the generation of sequences towards a preference for either the initiator or TATA-box motif distribution. This adaptability highlights the algorithm’s utility in fine-tuning the balance between different genetic motifs in the generated sequences.

6. Conclusion

In this study, we have introduced a cross-species DNA dataset (EPD-GenDNA). This establishes a new benchmark for generative models in DNA sequence synthesis. Our conditional DNA model has demonstrated its proficiency in producing species-specific sequences using this dataset.

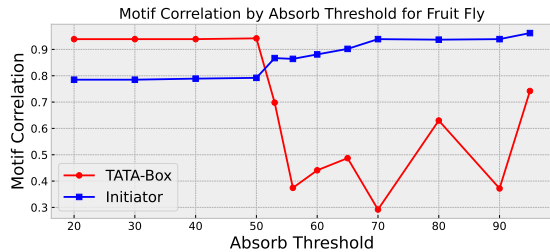


Figure 6. Tuning genetic motif preferences with varied absorbance thresholds, T_{absorb} . With the increment of T_{absorb} , the $Cor_{Initiator}$ for sequences refined by the Absorb-Escape shows an increase, while Cor_{TATA} fluctuates. An optimal T_{absorb} can be selected to achieve high values for both Cor_{TATA} and $Cor_{Initiator}$.

From a methodological perspective, we developed DiscDiff, a Latent Diffusion Model (LDM) specifically tailored for DNA generation. DiscDiff performs well on both conditional and unconditional DNA sequence generation tasks. Additionally, our Absorb-Escape algorithm effectively corrects mistakes made by diffusion models, significantly boosting the performance of DiscDiff on DNA generation. The versatility of our DiscDiff model extends beyond its current application, presenting the potential for testing in other types of discrete data and biological sequence generation tasks.

The Absorb-Escape algorithm demonstrates potential in harnessing the advantages of both diffusion and autoregressive models. We hope that researchers will leverage this to enhance sequence generation performance in tasks involving discrete data.

References

- Alamdari, S., Thakkar, N., van den Berg, R., Lu, A. X., Fusi, N., Amini, A. P., and Yang, K. K. Protein generation with evolutionary diffusion: sequence is all you need. *bioRxiv*, pp. 2023–09, 2023.
- Alipanahi, B., Delong, A., Weirauch, M. T., and Frey, B. J. Predicting the sequence specificities of dna-and rna-binding proteins by deep learning. *Nature biotechnology*, 33(8):831–838, 2015.
- Austin, J., Johnson, D. D., Ho, J., Tarlow, D., and Van Den Berg, R. Structured denoising diffusion models in discrete state-spaces. *Advances in Neural Information Processing Systems*, 34:17981–17993, 2021.
- Avdeyev, P., Shi, C., Tan, Y., Dudnyk, K., and Zhou, J. Dirichlet diffusion score model for biological sequence generation. *arXiv preprint arXiv:2305.10699*, 2023.
- Avsec, Ž., Agarwal, V., Visentin, D., Ledsam, J. R., Grabska-Barwinska, A., Taylor, K. R., Assael, Y., Jumper, J., Kohli, P., and Kelley, D. R. Effective gene expression prediction from sequence by integrating long-range interactions. *Nature methods*, 18(10):1196–1203, 2021.
- Brown, T., Mann, B., Ryder, N., Subbiah, M., Kaplan, J. D., Dhariwal, P., Neelakantan, A., Shyam, P., Sastry, G., Askell, A., et al. Language models are few-shot learners. *Advances in neural information processing systems*, 33:1877–1901, 2020.
- Chen, T., Zhang, R., and Hinton, G. Analog bits: Generating discrete data using diffusion models with self-conditioning. *arXiv preprint arXiv:2208.04202*, 2022.
- Dalla-Torre, H., Gonzalez, L., Mendoza-Revilla, J., Caranza, N. L., Grzywaczewski, A. H., Oteri, F., Dallago, C., Trop, E., de Almeida, B. P., Sirelkhatim, H., et al. The nucleotide transformer: Building and evaluating robust foundation models for human genomics. *bioRxiv*, pp. 2023–01, 2023.
- Dhariwal, P. and Nichol, A. Diffusion models beat gans on image synthesis. *Advances in neural information processing systems*, 34:8780–8794, 2021.
- Dieleman, S., Sartran, L., Roshannai, A., Savinov, N., Ganin, Y., Richemond, P. H., Doucet, A., Strudel, R., Dyer, C., Durkan, C., et al. Continuous diffusion for categorical data. *arXiv preprint arXiv:2211.15089*, 2022.
- Eraslan, G., Avsec, Ž., Gagneur, J., and Theis, F. J. Deep learning: new computational modelling techniques for genomics. *Nature Reviews Genetics*, 20(7):389–403, 2019.
- Goodfellow, I., Pouget-Abadie, J., Mirza, M., Xu, B., Warde-Farley, D., Ozair, S., Courville, A., and Bengio, Y. Generative adversarial nets. In Ghahramani, Z., Welling, M., Cortes, C., Lawrence, N., and Weinberger, K. (eds.), *Advances in Neural Information Processing Systems*, volume 27. Curran Associates, Inc., 2014.
- Grešová, K., Martinek, V., Čechák, D., Šimeček, P., and Alexiou, P. Genomic benchmarks: a collection of datasets for genomic sequence classification. *BMC Genomic Data*, 24(1):25, 2023.
- Gu, A. and Dao, T. Mamba: Linear-time sequence modeling with selective state spaces. *arXiv preprint arXiv:2312.00752*, 2023.
- Gupta, A. and Zou, J. Feedback gan for dna optimizes protein functions. *Nature Machine Intelligence*, 1(2):105–111, 2019.
- Gupta, A., Yu, L., Sohn, K., Gu, X., Hahn, M., Fei-Fei, L., Essa, I., Jiang, L., and Lezama, J. Photorealistic video generation with diffusion models. *arXiv preprint arXiv:2312.06662*, 2023.
- Han, X., Kumar, S., and Tsvetkov, Y. Ssd-lm: Semi-autoregressive simplex-based diffusion language model for text generation and modular control. *arXiv preprint arXiv:2210.17432*, 2022.
- Heusel, M., Ramsauer, H., Unterthiner, T., Nessler, B., and Hochreiter, S. Gans trained by a two time-scale update rule converge to a local nash equilibrium. *Advances in neural information processing systems*, 30, 2017.
- Ho, J., Salimans, T., Gritsenko, A., Chan, W., Norouzi, M., and Fleet, D. J. Video diffusion models, 2022. [URL https://arxiv.org/abs/2204.03458](https://arxiv.org/abs/2204.03458).
- Ho, J., Jain, A., and Abbeel, P. Denoising diffusion probabilistic models. *Advances in neural information processing systems*, 33:6840–6851, 2020.
- Ji, Y., Zhou, Z., Liu, H., and Davuluri, R. V. Dnabert: pre-trained bidirectional encoder representations from transformers model for dna-language in genome. *Bioinformatics*, 37(15):2112–2120, 2021.
- Kelley, D. R. Cross-species regulatory sequence activity prediction. *PLoS computational biology*, 16(7):e1008050, 2020.
- Kelley, D. R., Reshef, Y. A., Bileschi, M., Belanger, D., McLean, C. Y., and Snoek, J. Sequential regulatory activity prediction across chromosomes with convolutional neural networks. *Genome research*, 28(5):739–750, 2018.

- Killoran, N., Lee, L. J., DeLong, A., Duvenaud, D., and Frey, B. J. Generating and designing dna with deep generative models. *arXiv preprint arXiv:1712.06148*, 2017.
- Lal, A., Biancalani, T., and Eraslan, G. reglm: Designing realistic regulatory dna with autoregressive language models. In *NeurIPS 2023 Generative AI and Biology (GenBio) Workshop*, 2023.
- Li, X., Thickstun, J., Gulrajani, I., Liang, P. S., and Hashimoto, T. B. Diffusion-lm improves controllable text generation. *Advances in Neural Information Processing Systems*, 35:4328–4343, 2022.
- Li, Z., Das, A., Beardall, W. A., Zhao, Y., and Stan, G.-B. Genomic interpreter: A hierarchical genomic deep neural network with 1d shifted window transformer. *arXiv preprint arXiv:2306.05143*, 2023.
- Lin, Z., Gong, Y., Shen, Y., Wu, T., Fan, Z., Lin, C., Chen, W., and Duan, N. Genie: Large scale pre-training for text generation with diffusion model. *arXiv preprint arXiv:2212.11685*, 2022.
- Liu, H., Chen, Z., Yuan, Y., Mei, X., Liu, X., Mandic, D., Wang, W., and Plumbley, M. D. Audioldm: Text-to-audio generation with latent diffusion models. *arXiv preprint arXiv:2301.12503*, 2023.
- Liu, J., Fu, M., Wang, M., Wan, D., Wei, Y., and Wei, X. Cancer vaccines as promising immuno-therapeutics: platforms and current progress. *Journal of Hematology & Oncology*, 15(1):28, 2022.
- Lovelace, J., Kishore, V., Wan, C., Shekhtman, E., and Weinberger, K. Q. Latent diffusion for language generation. *arXiv preprint arXiv:2212.09462*, 2022.
- Lu, C., Zhou, Y., Bao, F., Chen, J., Li, C., and Zhu, J. Dpm-solver: A fast ode solver for diffusion probabilistic model sampling in around 10 steps. *Advances in Neural Information Processing Systems*, 35:5775–5787, 2022.
- McInnes, L., Healy, J., and Melville, J. Umap: Uniform manifold approximation and projection for dimension reduction. *arXiv preprint arXiv:1802.03426*, 2018.
- Metz, L., Poole, B., Pfau, D., and Sohl-Dickstein, J. Unrolled generative adversarial networks. *arXiv preprint arXiv:1611.02163*, 2016.
- Meylan, P., Dreos, R., Ambrosini, G., Groux, R., and Bucher, P. Epd in 2020: enhanced data visualization and extension to ncna promoters. *Nucleic Acids Research*, 48(D1):D65–D69, 2020.
- Mock, F., Kretschmer, F., Kriese, A., Böcker, S., and Marz, M. Taxonomic classification of dna sequences beyond sequence similarity using deep neural networks. *Proceedings of the National Academy of Sciences*, 119(35):e2122636119, 2022.
- Nguyen, E., Poli, M., Faizi, M., Thomas, A., Birch-Sykes, C., Wornow, M., Patel, A., Rabideau, C., Massaroli, S., Bengio, Y., et al. Hyenadna: Long-range genomic sequence modeling at single nucleotide resolution. *arXiv preprint arXiv:2306.15794*, 2023.
- Périer, R. C., Junier, T., and Bucher, P. The eukaryotic promoter database epd. *Nucleic acids research*, 26(1): 353–357, 1998.
- Preechakul, K., Chatthee, N., Wizadwongsa, S., and Suwajanakorn, S. Diffusion autoencoders: Toward a meaningful and decodable representation. In *Proceedings of the IEEE/CVF Conference on Computer Vision and Pattern Recognition*, pp. 10619–10629, 2022.
- Radford, A., Wu, J., Child, R., Luan, D., Amodei, D., Sutskever, I., et al. Language models are unsupervised multitask learners. *OpenAI blog*, 1(8):9, 2019.
- Rombach, R., Blattmann, A., Lorenz, D., Esser, P., and Ommer, B. High-resolution image synthesis with latent diffusion models. In *Proceedings of the IEEE/CVF conference on computer vision and pattern recognition*, pp. 10684–10695, 2022.
- Ronneberger, O., Fischer, P., and Brox, T. U-net: Convolutional networks for biomedical image segmentation. In *Medical Image Computing and Computer-Assisted Intervention—MICCAI 2015: 18th International Conference, Munich, Germany, October 5-9, 2015, Proceedings, Part III 18*, pp. 234–241. Springer, 2015.
- Salimans, T., Karpathy, A., Chen, X., and Kingma, D. P. Pixelcnn++: Improving the pixelcnn with discretized logistic mixture likelihood and other modifications. *arXiv preprint arXiv:1701.05517*, 2017.
- Sohl-Dickstein, J., Weiss, E., Maheswaranathan, N., and Ganguli, S. Deep unsupervised learning using nonequilibrium thermodynamics. In *International conference on machine learning*, pp. 2256–2265. PMLR, 2015.
- Song, J., Meng, C., and Ermon, S. Denoising diffusion implicit models. *arXiv preprint arXiv:2010.02502*, 2020a.
- Song, Y., Sohl-Dickstein, J., Kingma, D. P., Kumar, A., Ermon, S., and Poole, B. Score-based generative modeling through stochastic differential equations. *arXiv preprint arXiv:2011.13456*, 2020b.
- Taskiran, I. I., Spanier, K. I., Dickmanken, H., Kempynck, N., Pančíková, A., Ekşi, E. C., Hulselmans, G., Ismail, J. N., Theunis, K., Vandepoel, R., et al. Cell type directed design of synthetic enhancers. *Nature*, pp. 1–3, 2023.

- Touvron, H., Lavril, T., Izacard, G., Martinet, X., Lachaux, M.-A., Lacroix, T., Rozière, B., Goyal, N., Hambro, E., Azhar, F., et al. Llama: Open and efficient foundation language models. *arXiv preprint arXiv:2302.13971*, 2023.
- Vahdat, A., Kreis, K., and Kautz, J. Score-based generative modeling in latent space. *Advances in Neural Information Processing Systems*, 34:11287–11302, 2021.
- Vaswani, A., Shazeer, N., Parmar, N., Uszkoreit, J., Jones, L., Gomez, A. N., Kaiser, Ł., and Polosukhin, I. Attention is all you need. *Advances in neural information processing systems*, 30, 2017.
- Wang, Y., Wang, H., Wei, L., Li, S., Liu, L., and Wang, X. Synthetic promoter design in escherichia coli based on a deep generative network. *Nucleic Acids Research*, 48(12):6403–6412, 2020.
- Watson, J. L., Juergens, D., Bennett, N. R., Trippe, B. L., Yim, J., Eisenach, H. E., Ahern, W., Borst, A. J., Ragotte, R. J., Milles, L. F., et al. De novo design of protein structure and function with rfdiffusion. *Nature*, 620(7976):1089–1100, 2023.
- Xia, G., Danier, D., Das, A., Fotiadis, S., Nabiei, F., Sengupta, U., and Bernacchia, A. Score normalization for a faster diffusion exponential integrator sampler. 2023. URL <https://openreview.net/forum?id=CZ0lnMcUVw>.
- Xu, J., Liu, X., Yan, J., Cai, D., Li, H., and Li, J. Learning to break the loop: Analyzing and mitigating repetitions for neural text generation. *Advances in Neural Information Processing Systems*, 35:3082–3095, 2022.
- Zhang, Q. and Chen, Y. Fast sampling of diffusion models with exponential integrator. In *The Eleventh International Conference on Learning Representations*, 2023. URL <https://openreview.net/forum?id=Loek7hfb46P>.
- Zhang, Y., Gu, J., Wu, Z., Zhai, S., Susskind, J., and Jaitly, N. Planner: Generating diversified paragraph via latent language diffusion model. *arXiv preprint arXiv:2306.02531*, 2023.
- Zhou, J. and Troyanskaya, O. G. Predicting effects of noncoding variants with deep learning-based sequence model. *Nature methods*, 12(10):931–934, 2015.
- Zrimec, J., Fu, X., Muhammad, A. S., Skrekas, C., Jauniskis, V., Speicher, N. K., Börlin, C. S., Verendel, V., Chehreghani, M. H., Dubhashi, D., et al. Controlling gene expression with deep generative design of regulatory dna. *Nature communications*, 13(1):5099, 2022.

A. Dataset Preparation

Table 7. The statistics of EPDnew dataset.

	# Unique Values	Examples
genes	130,014	CAACAAGGCACAGCAC...
promoters	159,125	GGCCCGTTTTTTAAT...
cell types	2713	[Esophageal Epithelial Cells, Hippocampus, ...]
gene function description	130,014	[AHSP:alpha hemoglobin stabilizing protein, ...]
species	15	[Homo sapiens (Human), Zea mays (corn), ...]
expression levels	29,349,475	[250,264,338, ...]
transcription starting site	29,349,475	[10,0,-1, ...]

Source Description The European Promoter Database (EPD) is a vital tool for biologists, with a primary focus on gathering and categorising promoters of eukaryotes. The EPD comprises promoter data sourced from numerous published articles. The EPDnew database, or High-Throughput EPD (HT-EPD), provides an even more comprehensive and rigorous dataset. The EPDnew has been enhanced by combining conventional EPD promoters with in-house analyses of promoter-specific high-throughput data, albeit for only selected organisms. This strategy enhances the precision and commendable coverage of EPDnew. It’s worth noting that the evidence used in EPDnew primarily arises from Transcription Start Site (TSS) mapping derived from high-throughput experiments, notably CAGE and Oligocapping.

Data Selection Data was obtained from the EPDnew database without any exclusions, allowing for the incorporation of all available samples and associated promoters. Sequences between -1024 and +1023 base pairs from the transcription start site were chosen, ensuring a total length of 2048 base pairs - a convenient choice due to its alignment to powers of 2. This range covers crucial promoter elements like GC and TATA boxes, and also allows the algorithm to identify any possible hidden patterns and interconnections preceding and succeeding the transcription start site.

Time Frame The temporal aspect of our data is not limited to a specific time frame or year. The data was collected entirely as of August 2023.

Data collection and preprocessing Data collection started by manually downloading data files through FTP, followed by accessing fasta data via the website’s graphical interface. Carefully extracted metadata from Python scripts was then integrated with promoter sequences to form a comprehensive table.

Given the species-specific fragmentation of the acquired data, an iterative method aided in bringing together diverse FASTA files into one consistent table, with important attributes such as ‘kingdom’ and ‘species’ integrated into the DataFrame at extraction. A crucial pre-processing step involved categorising DNA sequences as ‘upstream’ or ‘downstream’ based on their relative positioning. Normalisation and transformation techniques were implemented where necessary to ensure data uniformity and integrity were maintained.

Simultaneously, an additional dataset containing gene expression data underwent similar aggregation processes. Promoter expression sample data was synchronised with the main DataFrame. To optimize data storage and retrieval, the processed data was archived as a Pickle file.

Data integration and duplicate removal processes were also undertaken. Subsequently, the integrity and consistency of the data have been validated through multiple checks, including the verification of value counts for specific columns and a comparison of the data against EPDnew statistics.

Data Variables

- Promoter Sequences: -1024 to 1023 bp from tss
- PID: A unique identifier for each promoter in the EPDnew database.
- Species: one of 15 species in our dataset

- Average Expression Value: mean of expression values of every sample pertaining to a specified EPDnew promoter
- Sample Name: Encompasses details like cell line and environmental conditions.
- Gene Description: description of gene function of the gene the promoter is regulating

Data Size and Structure As shown in Table 7, the data set we compiled from EPDnew comprises of 159,125 distinct promoter sequences derived from 15 eukaryotic species, which are connected to 130,014 individual genes. Most of these genes have gene function definitions associated with them in the gathered data. The promoters have experimental expression levels and co-determined transcription start sites associated with them. These are frequently recorded in various cell types per promoter and might hold many experimental values for a single cell type. Our methodically structured dataset is in tabular form, facilitating smooth and comprehensive accessibility and manipulation for in-depth analysis.

B. Justification of Two-Stage Training

The separation of VAE and the denoising model training can be justified by the loss function of LSGM (Vahdat et al., 2021). LSGM jointly trains a VAE and the denoising model with a training loss consisting of a reconstruction term and KL divergence between encoder distribution $p(z_0|x)$ and the prior distribution of the latent variable $p(z_0)$. The latter term can be expressed in terms of the score function $S_\theta(x(t),t)$. The optimisation of this loss is challenging, requiring different weighting mechanisms for the training objective and variance reduction techniques for stability. The separation of training is equivalent to a special training schedule with the KL divergence term being fixed in the first stage, and then training the denoising model in the second stage. The performance gain of separating the training process has been shown in the image generation domain (Rombach et al., 2022; Preechakul et al., 2022). In the section below, we provide the empirical evaluation of this method for DNA sequence generation.

C. U-Net Configuration

U-Net is trained by sampling t from uniform distribution $U[1,T]$ and ε from $\mathcal{N}(\mathbf{0},I)$. We adopted the U-Net backbone from LDM (Ho et al.; Liu et al., 2023; Ronneberger et al., 2015) to implement $\varepsilon_\theta(z_t,t)$. Cross-attention (Rombach et al., 2022) is added to each layer to enable the integration of conditional information, and self-attention (Vaswani et al., 2017) is added to the middle layers to improve the expressive power of the network.

The UNet model used consists of four down and four up blocks. Each block consists of eight sequential ResNet blocks, followed by a single upsampling or downsampling block to change the number of channels. The third down block and the second up block are enriched with cross-attention layers, one applied after each ResNet block.

Each ResNet block transforms an input tensor through operational layers including normalisation, swish non-linearity, upsampling, two convolutional layers and time-embedding projection, culminating in an output tensor formed by summing the input tensor and the output of the second convolutional layer.

Attention layers, integral to the refinement of the feature representation, are incorporated in the third down and second up blocks, each consisting of eight 64-dimensional attention heads, executed by a scaled dot product attention mechanism without dropout and bias in the projection layers.

The UNet input and output contain 16 channels, each containing 16 x 16 arrays. The down blocks have channel dimensions of [256,256,512,512] and the up blocks mirror the encoder blocks in reverse order. In the forward process, we use $N = 1000$ steps. For EPD-GenDNA small, we reduce the embedding size to 8 x 8 x 8, and the other components of the U-Net are reduced proportionally.

D. Ablation VAE

D.1. VAE variants

CNN-VAE The convolutional VAE follows the encoder-decoder architecture. The encoder learns how to encode the discrete DNA sequence data into a continuous latent representation. Simultaneously, the decoder learns how to decode the latent representations into DNA sequence data in continuous space before it is quantised with ArgMax. A detailed illustration of the encoder architecture is in figure 7.

The decoder employs an architecture in symmetry with the encoder. In the decoder the same network layers are performed in reverse order and inverse operations are used in place of forward operations. Such inverse operation pairs include transposed convolution and convolution operation, upsampling and maxpooling operation.

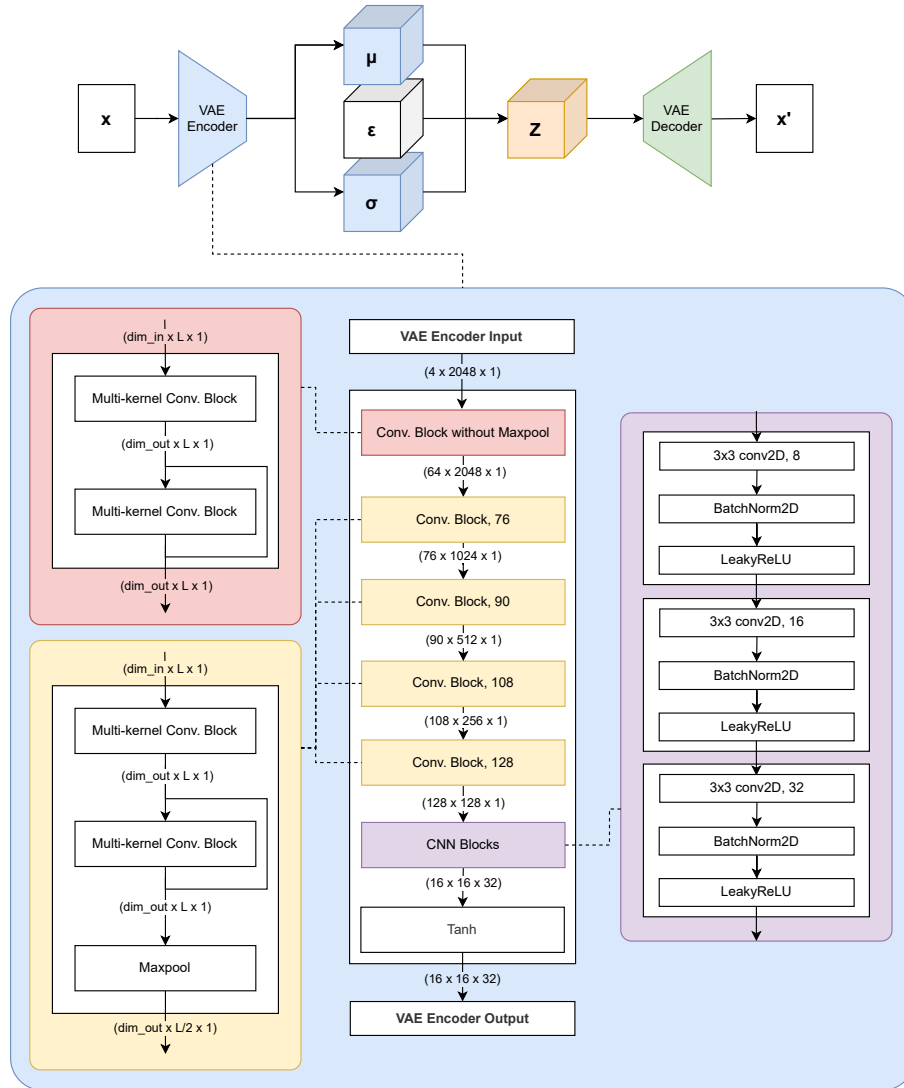


Figure 7. VAE Encoder Architecture

Two sections can be distinguished from the architecture: 1) the discrete data encoder (in red and yellow) and 2) the CNN Blocks (in purple)

The first section of the encoder encodes the one-hot encoded input into a 2-dimensional image-like representation. From the initial 4 channels due to one-hot encoding, the channel dimension is first increased to 64, then it increases further with steps of exponentially increasing number of kernels up to 128. This is implemented using Multi-kernel Convolution Blocks with perturbable kernel parameters combined with residual connections. By including a max-pooling layer in each layer, its length shrinks by powers of 2 to 128. This effectively expands our $4 \times 2048 \times 1$ data into $128 \times 128 \times 1$, an image-like surface when viewed along the channel and length. This stage of the encoder aims to capture high-level positional features along the length dimension via pooling, for each channel dimension of the DNA sequence by transforming from 1-dimensional features into a 2-dimensional surface.

The second section of the encoder uses a CNN architecture for learning latent representations. There are three layers of the CNN block, each performing 3×3 kernel on the channel-length surface followed by BatchNorm2D and LeakyReLU activation. The CNN block in the encoder learns to produce different feature maps of size 16×16 from the 128×128 surface, which are concatenated into a 3-dimensional latent representation of shape $16 \times 16 \times 32$, effectively increasing the width dimension. The latent representation can be partitioned into two blocks of size $16 \times 16 \times 16$, representing the mean and log-variance of the learned features. Assuming priors of diagonal Gaussian distributions, we can take samples from the standard Gaussian distribution and use the reparameterisation trick to optimise for the variational learning.

The Multi-kernel Convolution Block is the elementary building block in the first section of the VAE network. The block is structured to first perform normalisation and activation first, then conv1D operations are performed on a list of kernel sizes, where the results are then concatenated. An example Multi-kernel Convolution Block with the list of kernel sizes $[1, 3, 5]$ is illustrated in figure 8.

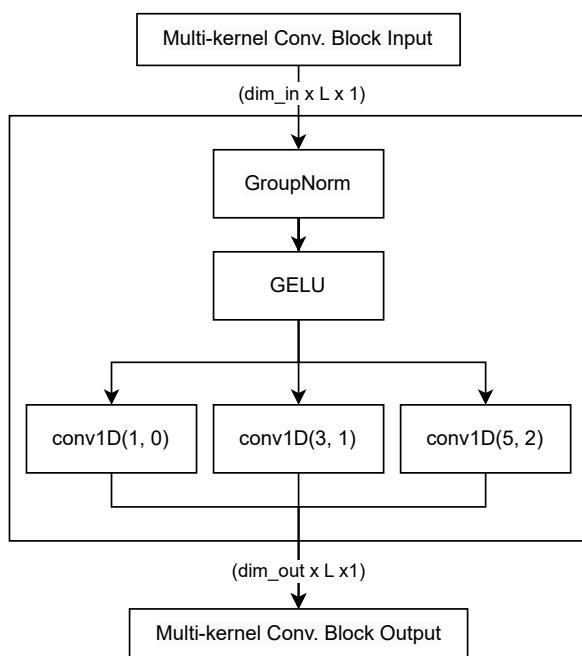


Figure 8. An Example of Multi-kernel Convolution Block

CNN-Attn-VAE For CNN-Attn-VAE, we replace the first stage encoder of the VAE encoder with CNNs and self-attention layers as used in Enformer (Avsec et al., 2021) for genomic assay prediction.

1D-Swin-VAE For 1D-Swin-VAE, we replace the first stage encoder of the VAE encoder with 1-d Swin (Li et al., 2023), a type of sparse transformer for genomic sequence modelling.

D.2. Embedding Space Analysis

Here, we explore the embedding space of three encoders. Appendix D.2 shows the latent distance embedding of three encoders with UMAP (McInnes et al., 2018). Note that while the species information is not given during the training of VAE,

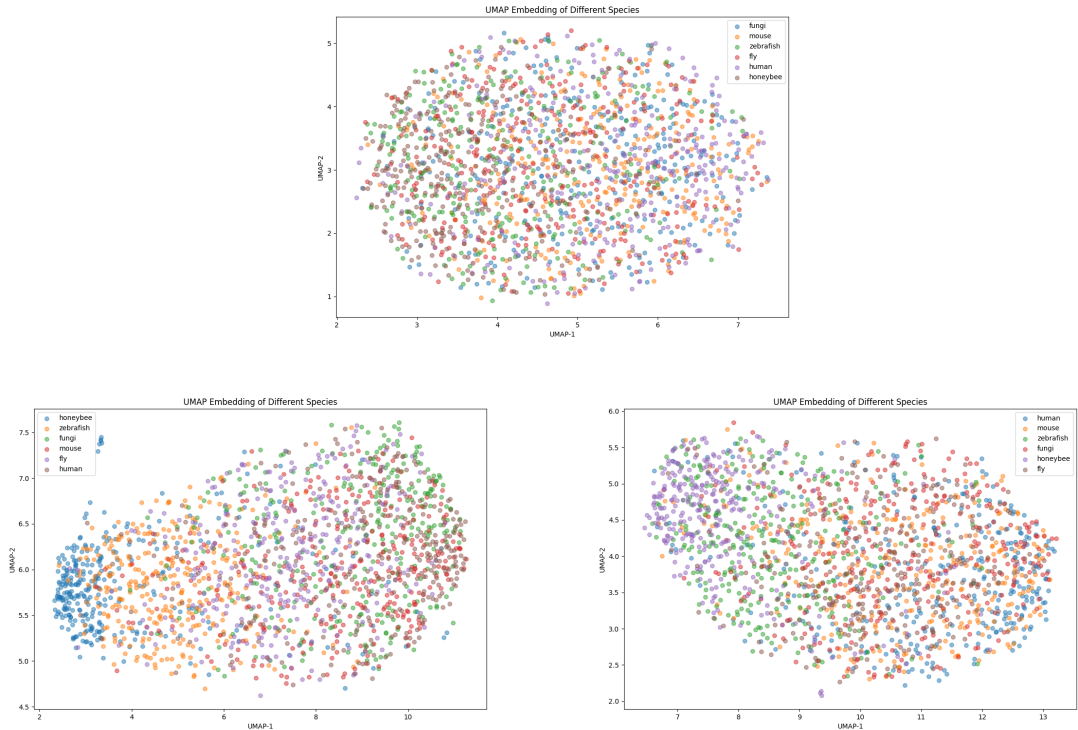


Figure 9. The top one is the latent space of CNN-VAE, while the bottom left is for CNN-Attn-VAE and the bottom right is 1D-Swin-VAE, respectively.

it can be seen that while the data points in the embedding space of 1D-Swin-VAE and CNN-Attn-VAE automatically cluster into species, the embedding space from CNN-VAE doesn't cluster. While this behaviour could be useful for unsupervised learning, it has the potential to increase the complexity of the learnt embedding space. Hereby, it may make the learning process in the second stage of LDM more challenging, resulting in lower-quality examples. The complexity of the embedding space can also be measured by the number of components required to recover 95% of the variance in the original dataset with PCA. For two models: 1D-Swin-VAE and CNN-VAE which archive relatively the same amount of reconstruction accuracy. CNN-VAE requires 1312 components to recover the 95% variance, while 1D-swin-VAE requires 1342 components.

E. DiscDiff and Baseline Models

DiscDiff Training The model was trained utilizing the NVIDIA RTX A6000 graphics card. During the first stage, a Variational Autoencoder (VAE) was trained on a dataset comprising 160,000 sequences spanning 15 different species. This training was executed over 24 GPU hours with the primary goal of accurately reconstructing the input sequences. The chosen learning rate was 0.0001, paired with the Adam Optimizer. A batch size of 128 was set, and the KL divergence weight was determined at 10^{-4} . The resultant hidden representation, z , belongs to $\mathbb{R}^{16 \times 16 \times 16}$, which is precisely half the dimensionality of the original input $x \in \mathbb{R}^{4 \times 2048}$.

In the second training phase, a denoising UNet and other baselines were trained on NVIDIA A100 40GB with a fixed budget of 72 GPU-Hours. Given the GPU RAM capacity of 40 GB, we optimized the model by maximizing the number of residual blocks and self-attention layers. The training also incorporated a cosine learning scheduler, introducing a warm-up period for the initial 500 epochs. The learning rate was set at 0.00005, and a batch size of 256 was chosen for the training. DDPM (Ho et al., 2020) is used for sampling.

For a focused evaluation of the model's performance on unconditional generation, particularly in mammalian DNA sequence generation, we opted for a subset of the entire dataset. This subset includes sequences from *H. Sapiens* (human), *Rattus Norvegicus* (rat), *Macaca mulatta*, and *Mus musculus* (mouse), which collectively represent 50% of the total dataset.

Training on this subset not only streamlines the evaluation process but also allows for a more precise assessment of the generative algorithm’s efficacy and accuracy in producing mammalian sequences

Baselines The details about the **architecture and implementation** of the baseline models are as below:

- BitDiffusion (Chen et al., 2022): We enhance the current BitDiffusion implementation for DNA synthesis, originally from the DNA-Diffusion project¹, by expanding the models to encompass 380 million parameters. This network is composed of Convolutional Neural Networks (CNNs), interspersed with layers of cross-attention and self-attention.
- DDSM (Avdeyev et al., 2023): We scale up the original implementation of the denoising network used for promoter design in DDSM² to what is the corresponding size of the network given 470 million parameters. It is a convolution-based architecture with dilated convolution layers.
- D3PM (Austin et al., 2021): We take the implementation of D3PM for biological sequence generation from EvoDiff (Alamdari et al., 2023)³, adopting the algorithm for DNA generation. We use the original implementation of the denoising network, which has two versions: with sizes of 38M and 640M. We hereby have D3PM (small) and D3PM (big), respectively.
- Hyena (Nguyen et al., 2023): We modify the RegLM (Lal et al., 2023)⁴, a existing work uses hyena for DNA generation. Four pretrained Hyena models of different sizes (hyenadna-large-1m-seqlen, hyenadna-medium-160k0seqlen, heynadna-small-32k-seqlen, and hyenaana-tiny-16k-seqlen-d128) are downloaded from HuggingFace⁵ and used for full-size fine-tuning, we apply the fine-tuned models for generations on EPD-GenDNA.

¹<https://github.com/pinellolab/DNA-Diffusion>

²<https://github.com/jzhoulab/ddsm>

³<https://github.com/microsoft/evodiff>

⁴<https://github.com/Genentech/regLM>

⁵<https://huggingface.co/LongSafari>

F. Additional Results

We provide additional results for conditional generations on EPD-GenDNA-small dataset below. Table 14 provides the unconditional generation results for Hyena models together with other models.

Model	Baking Yeast		Chicken		Corn	
	TATA \uparrow	Initiator \uparrow	TATA \uparrow	Initiator \uparrow	TATA \uparrow	Initiator \uparrow
Hyena	0.958	0.723	0.956	0.553	0.995	0.875
DiscDiff	0.858	0.824	0.960	0.683	0.983	0.796
Absorb-Escape	0.864	0.902	0.910	0.625	0.991	0.824

Table 8. Conditional Generations on EPD-GenDNA-small: for human, honee, and baking yeast.

Model	Dog		Elegans		Fission Yeast	
	TATA \uparrow	Initiator \uparrow	TATA \uparrow	Initiator \uparrow	TATA \uparrow	Initiator \uparrow
Hyena	0.890	0.130	0.930	0.592	0.929	0.320
DiscDiff	0.829	0.167	0.677	0.947	0.860	0.139
Absorb-Escape	0.754	0.527	0.857	0.428	0.947	0.412

Table 9. Conditional Generations on EPD-GenDNA-small: for human, honey bee, and baking yeast.

Model	Fruit Fly		Honey Bee		Human	
	TATA \uparrow	Initiator \uparrow	TATA \uparrow	Initiator \uparrow	TATA \uparrow	Initiator \uparrow
Hyena	0.970	0.198	0.933	0.779	0.922	0.263
DiscDiff	0.813	0.926	0.897	0.924	0.908	0.579
Absorb-Escape	0.937	0.630	0.905	0.771	0.900	0.411

Table 10. Conditional Generations on EPD-GenDNA-small: for human, honey bee, and baking yeast.

Model	Macaque		Mouse		Plasmodium	
	TATA \uparrow	Initiator \uparrow	TATA \uparrow	Initiator \uparrow	TATA \uparrow	Initiator \uparrow
Hyena	0.935	0.641	0.959	0.463	0.792	-0.284
DiscDiff	0.939	0.700	0.941	0.628	0.888	-0.686
Absorb-Escape	0.949	0.745	0.930	0.471	0.853	-0.419

Table 11. Conditional Generations on EPD-GenDNA-small: for human, honey bee, and baking yeast.

Model	Rat		Thale Cress		Zebrafish	
	TATA \uparrow	Initiator \uparrow	TATA \uparrow	Initiator \uparrow	TATA \uparrow	Initiator \uparrow
Hyena	0.972	0.492	0.979	0.918	0.969	0.664
DiscDiff	0.939	0.618	0.970	0.697	0.953	0.773
Absorb-Escape	0.975	0.671	0.994	0.893	0.985	0.594

Table 12. Conditional Generations on EPD-GenDNA-small: for human, honey bee, and baking yeast.

DiscDiff: Latent Diffusion Model for DNA Sequence Generation

Encode	Acc	S-FID ↓	Cor _{TATA} ↑	ΔDiv ↓
CNN-VAE	99.4 %	45.2	0.858	4.2%
CNN-Attn-VAE	98.8 %	53.6	0.531	9.8%
1D-Swin-VAE	99.6 %	82.1	0.651	7.5%

Table 13. Unconditional Generations: Comparison of different version of DiscDiff on EPD-GenDNA-large.

Model	EPD-GenDNA-small			EPD-GenDNA-large		
	S-FID ↓	Cor _{TATA} ↑	Div ↑	S-FID ↓	Cor _{TATA} ↑	Div ↑
Random (Reference)	119.0	-0.241	0.828	106.0	0.030	0.261
Sample from Training Set	0.509	1.0	0.535	0.100	0.999	0.131
VAE	295.0	-0.167	0.531	250.0	0.007	0.025
BitDiffusion	405	0.058	0.086	100.0	0.066	0.111
D3PM (small)	97.4	0.0964	0.815	94.5	0.363	0.259
D3PM (large)	161.0	-0.208	0.534	224.0	0.307	0.132
DDSM (Time Dilation)	504.0	0.897	0.129	1113.0	0.839	0.001
DiscDiff (Ours)	57.4	0.973	0.491	45.2	0.858	0.173
Hyena (Tiny)	2.97	0.972	0.535	3.34	0.940	0.141
Hyena (Small)	3.20	0.913	0.530	1.16	0.924	0.136
Hyena (Middle)	2.13	0.769	0.538	2.54	0.925	0.141
Hyena (Large)	1.76	0.952	0.558	1.51	0.887	0.138
Absorb-Escape (Ours)	3.21	0.975	0.478	4.38	0.892	0.150

Table 14. Unconditional Generations: Comparison of models on EPD-GenDNA-small and EPD-GenDNA-large.

G. Motif Distributions for 15 species

We plot TATA-box, GC content, Initiator, and CCAAT-box for 15 species as below.



Figure 10. Baking Yeast



Figure 11. Chicken



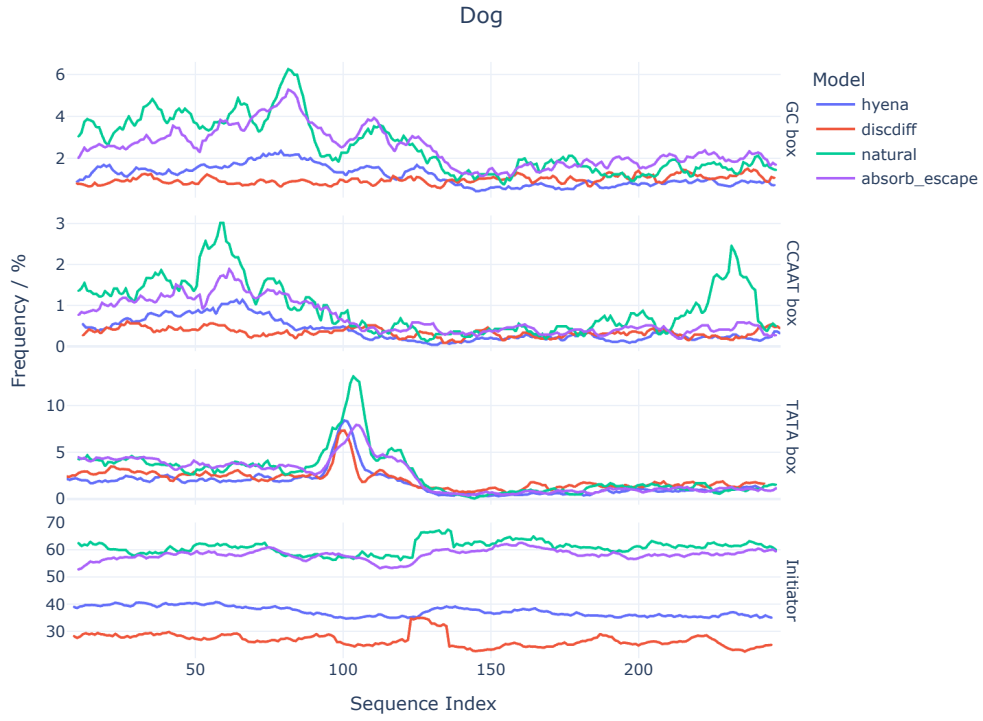


Figure 14. dog

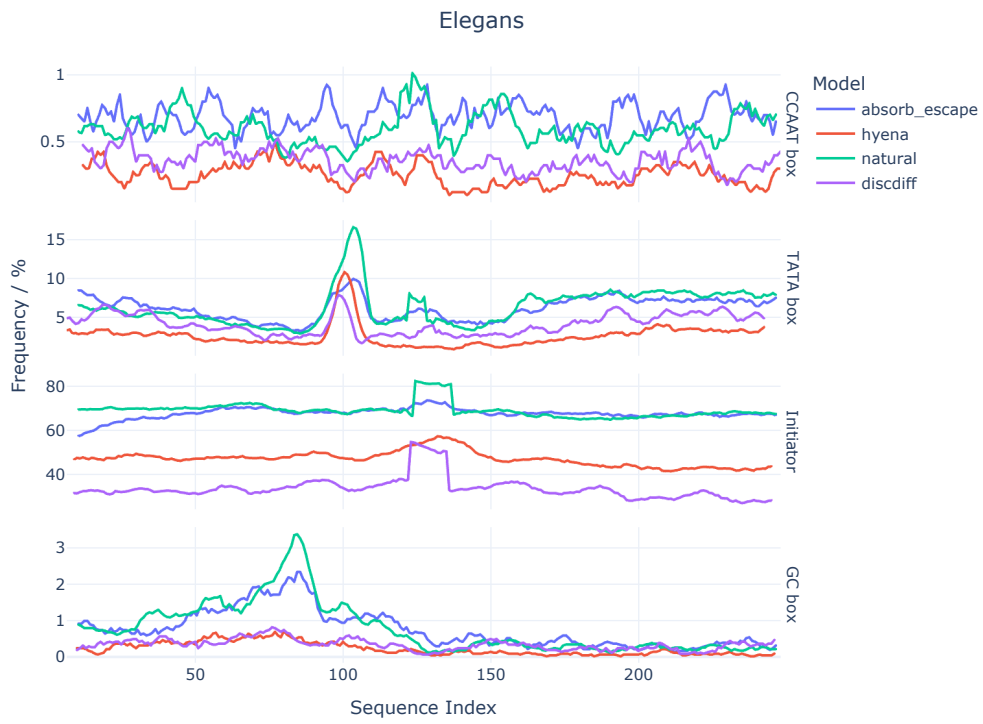


Figure 15. elegans

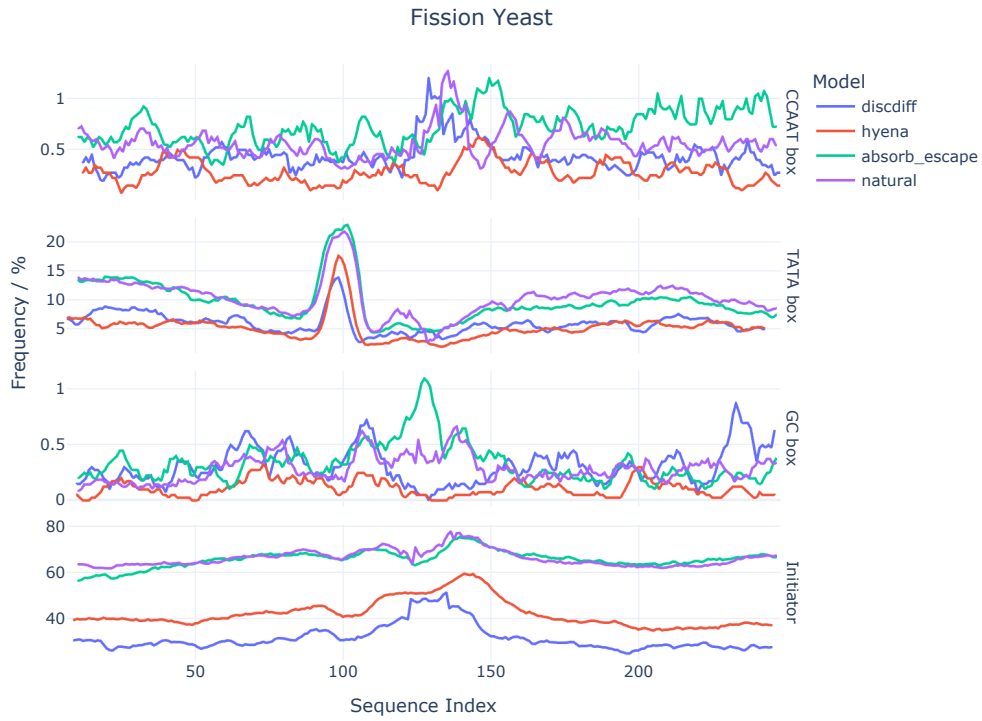


Figure 16. fission yeast

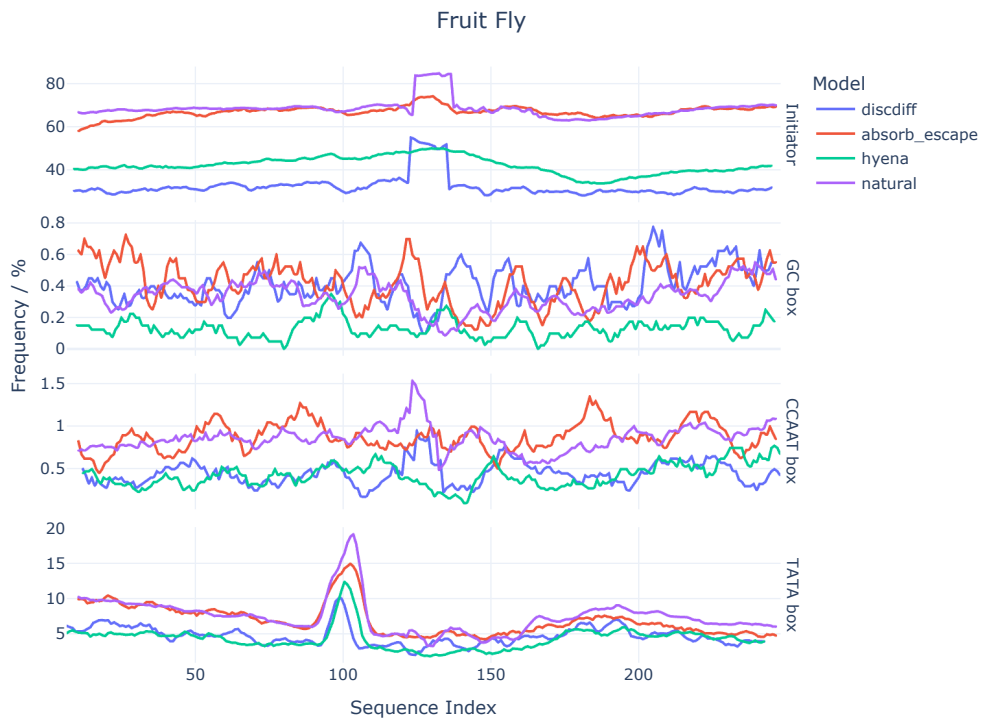


Figure 17. fruit fly

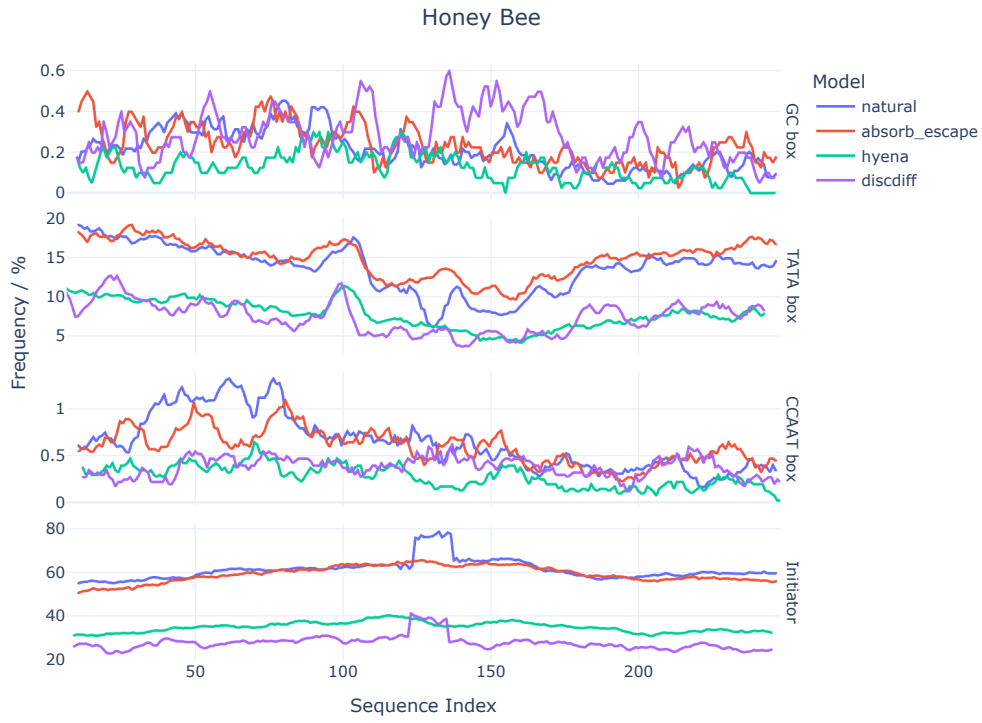


Figure 18. honey bee

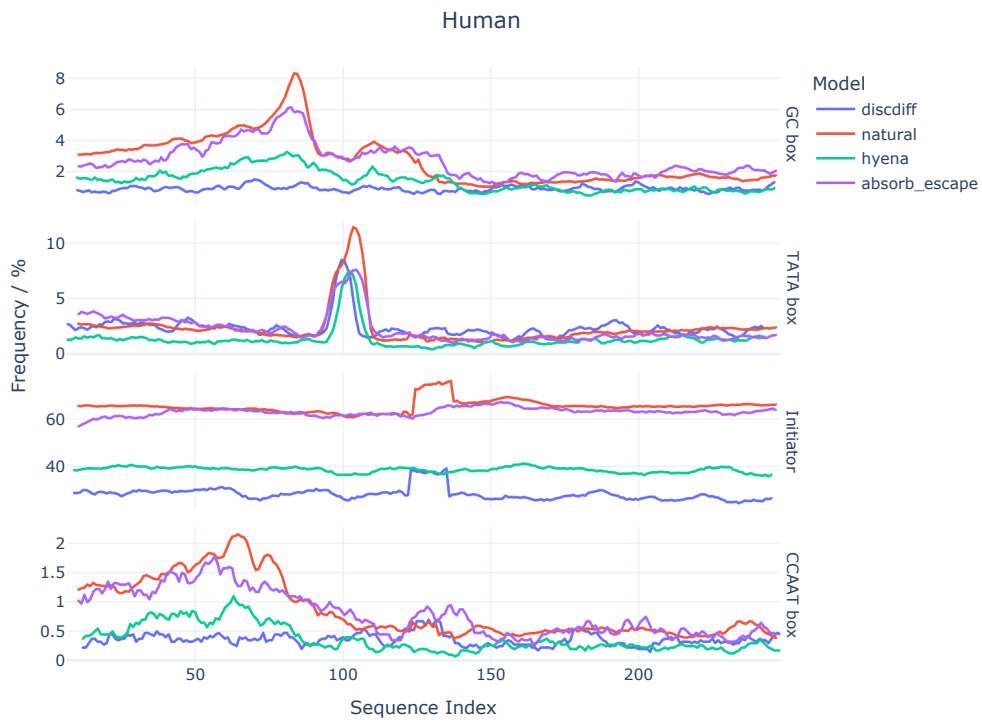


Figure 19. human

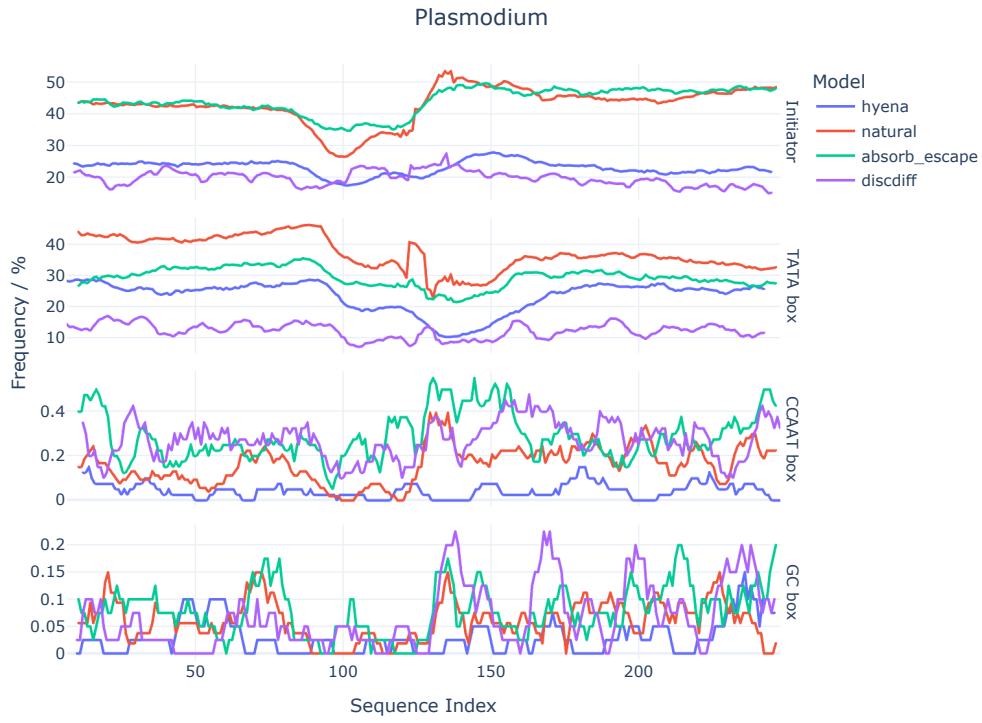


Figure 20. plasmodium

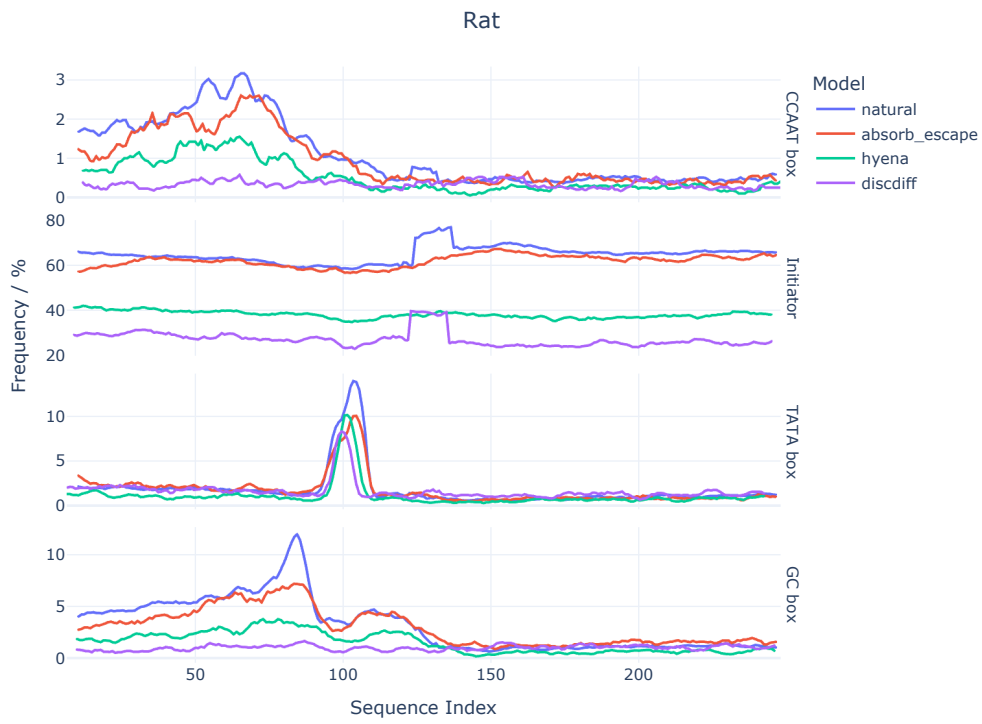


Figure 21. rat



Figure 22. thale cress



Figure 23. macaque

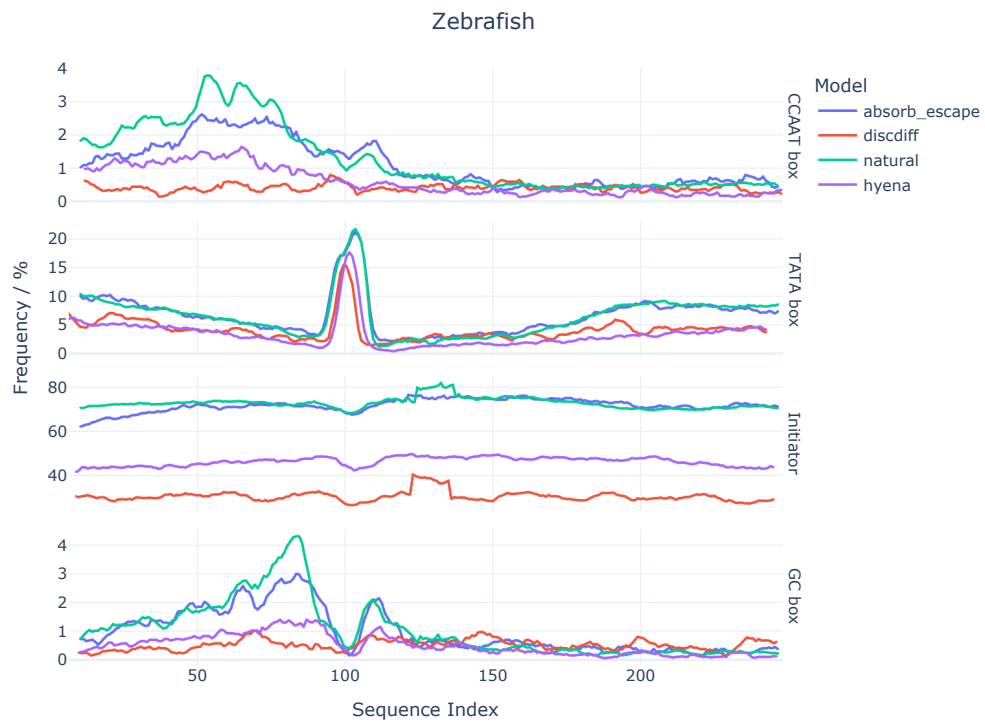


Figure 24. zebrafish